



# Fabrication of a High Chromium Cast Iron/Low Carbon Steel Bimetal: Diffusion Behavior and Bonding Strength

Yongcun Li, Jing Gao, Na Xu, Ping Li, Mengying Gong, and Weiping Tong

(Submitted December 9, 2018; in revised form September 15, 2019; published online October 25, 2019)

In the present study, a high chromium cast iron (HCCI) alloyed with Mo (16 wt.% Cr-6 wt.% Mo-2.4 wt.% C) with excellent wear resistance was bonded to a low carbon steel (LCS) by surface liquid-phase sintering. The bimetal was also subjected to a quenching + tempering treatment. The diffusion behavior of the atoms between the HCCI and LCS was analyzed. The bonding strength of the bimetal was investigated before and after heat treatment. The results show that the bimetal had a good bonding quality due to the uphill diffusion of C atoms. A diffusion zone with a width of approximately 37  $\mu\text{m}$  and a troostite structure formed on the HCCI side by the interface. With different bonding times, there was no obvious change in the width of the diffusion zone. The shear strength of the bimetal at all holding times was reduced from a high level after heat treatment and decreased with increasing tempering temperature. The impact toughness of the bimetal substantially increased compared with that of the HCCI. After a quenching treatment, the impact toughness of the bimetal decreased, and the microhardness of the diffusion zone improved. As the tempering temperature increased, the microhardness and impact toughness decreased and increased, respectively.

**Keywords** bimetal, bonding strength, diffusion, heat treatment, high chromium cast iron

## 1. Introduction

High chromium cast irons (HCCIs) have been widely used in various industries, such as in cement manufacturing and for mining machinery, due to their excellent wear resistance (Ref 1-4). Some researchers have demonstrated that the performance of HCCIs could be improved by the addition of Mo (Ref 5-7), and quenching + high temperature tempering treatment has consistently been used to improve their strength and wear resistance (Ref 8-10).

Low carbon steels (LCSs) or low alloy steels (LASs) have the disadvantages of poor corrosion resistance and insufficient wear resistance, resulting in the reduction of their service life. To overcome these shortcomings, bimetals have gradually become a research priority (Ref 11-22), and researchers have attempted to bond HCCIs to LCSs or LASs (Ref 13-20). X. Xiao fabricated a HCWCI/carbon steel bimetal liner using the liquid-liquid compound lost foam casting method, and the interface of the liner presented an excellent metallurgical bonding state (Ref 15). Xiong bonded the HCCI to a medium

carbon steel by liquid-solid casting with and without an electromagnetic induction field, and metallurgical bonding with a good interface was obtained by the diffusion of atoms (Ref 16, 17). Kurt investigated the effects of bonding temperature and holding time on the interface microstructure and bonding strength and concluded that high bonding temperature and long holding time have a positive influence on bonding quality (Ref 18, 19). Gao et al. (Ref 21) developed a HCCI/LCS bimetal by hot diffusion-compression bonding, and the bond strength was improved by increasing the temperature and reducing the strain rate. In our previous work (Ref 22), the uphill diffusion of C atoms was found during the bonding process of a diffusion couple consisting of HCCI and LCS.

Surface liquid-phase sintering (Ref 23) is a method that places the premade powder on the surface of the substrate and heats it to achieve metallurgical mixing by the diffusion of atoms in a vacuum or under inert gas protection. As a novel preparation method, it has the following advantages. As a continuous and dense HCCI, its microstructure has fewer defects, such as cracks and voids, which can play a role in improving corrosion resistance and wear resistance. The microstructure of the HCCI can be adjusted to accommodate the requirements of the working conditions by appropriately designing the chemical component of the premade powders. During the incubation process, sufficient atomic diffusion between the HCCI and substrate material can be achieved to obtain a good bonding strength. In our previous work, 6 wt.% Mo was added into a HCCI (16 wt.% Cr-2.4 wt.% C), and the wear resistance was substantially improved via a quenching + tempering treatment, but the alloyed HCCI showed poor toughness (Ref 24). In the present study, the alloyed HCCI was bonded to the LCS by surface liquid-phase sintering to improve toughness. The influence of heat treatment on the bonding strength of the bimetal was studied systematically. The diffusion behavior of atoms between the HCCI and LCS was also investigated in detail.

**Yongcun Li, Jing Gao, Na Xu, Ping Li, Mengying Gong, and Weiping Tong.** Key Laboratory of Electromagnetic Processing of Materials, Northeastern University, Shenyang 110819, China. Contact e-mails: YC\_Lee1988@163.com, 467014557@qq.com, 346101182@qq.com, holidaybwping@163.com, gongmy1222@163.com, and wptong@mail.neu.edu.cn.

## 2. Materials and Methods

### 2.1 Materials

The LCS used as substrate material in the present study was a 20<sup>#</sup> gauge cold-rolled steel sheet with a thickness of 6 mm that was cut into a size of 120 mm × 80 mm by wire cutting. The LCS sheet was processed with a grinder and cleaned using alcohol to obtain chemically active surfaces. The prepared LCS sheet was placed into the bottom of an alumina crucible with the corresponding size.

Low-carbon ferrochromium, graphite and ferromolybdenum powders with particle sizes of 10-100 μm were used as raw materials for the sintering of the wear-resistant HCCI alloyed with Mo. The powders were uniformly mixed using a planetary mixer and loaded into the alumina crucible up to the LCS sheet. An argon gas protection furnace was used for the melting and in situ reaction of the raw material powders to avoid oxidation of the sample. The materials were heated to 1270 °C and held for 5 min, 20 min, and 40 min and then furnace cooled to room temperature. During the sintering process, the raw materials powders reacted at 1270 °C and formed a HCCI liquid alloy, and the processed LCS had a chemically active surface. Atomic diffusion occurred between LCS and HCCI to achieve good metallurgical bonding. The chemical compositions of LCS and obtained HCCI are listed in Table 1.

HCCI with a large thickness can be obtained by this method, and a schematic of the as-cast bimetal is shown in Fig. 1(a). To increase the strength, parts of the bimetal were heated to 1040 °C and held for 120 min to destabilize it and then the sample was cooled to room temperature with forced air. A tempering treatment was adopted to eliminate the residual stress in the samples caused by the forced-air cooling process where it was heated to 500, 550, and 600 °C, held for 120 min, and then

**Table 1 Chemical compositions of the HCCI and the LCS (wt.%)**

Material	C	Cr	Mo	Si	Mn	Ni	Fe
LCS	0.2	0.2	–	–	0.5	0.1	bal
HCCI	2.4	16.1	6.0	1.1-15	0.5-0.7	0.4-0.5	bal

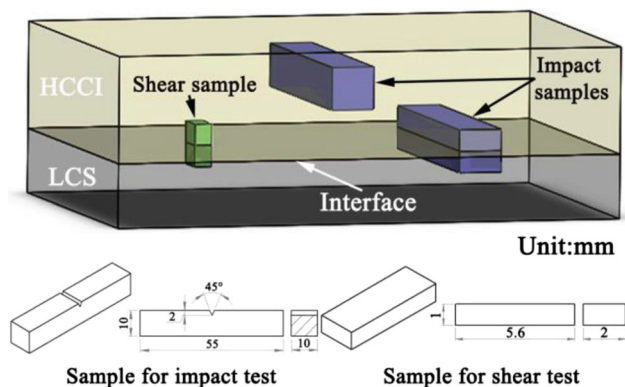


**Fig. 1** Positions and dimensions of samples for tests of impact toughness and shear strength

furnace cooled. The sample codes after the heat treatments are shown in Table 2.

### 2.2 Microstructural Analysis

Samples for metallography were cut into a size of 10 mm × 10 mm × 10 mm across the interface of the bimetal, ground with 60–2000# grinder papers, and then polished using a 1 μm diamond polishing paste. A reagent of 4 vol.% nital was used for etching of samples. The microstructure was investigated with optical microscopy (OM) on an OLYMPUS-GX71 instrument and field emission scanning electron microscopy (FE-SEM) on an Ultra Plus (ZEISS) instrument. The diffusion of the atoms between the HCCI and LCS was analyzed by electron-probe microanalysis (EPMA) on a JXA-8530F instrument. A TECNAI G20 TEM equipped with an Oxford<sup>®</sup> Inca EDS detector was utilized to investigate the microstructure of the diffusion zone and operated at 200 kV.

### 2.3 Microhardness, Impact and Shear Test

The hardness was measured using a Vickers hardness tester with a load of 200 g and a dwell time of 10 s, and the average value of 5 different measurements is reported. Impact testing was used to characterize the ability of the sample to resist an impact load by JAW-500 impact testing machine. According to the impact feature of the bimetal, a V-notch was processed on the LCS side. Shear strength was used to characterize the bonding strength of the HCCI and LCS. An instrument designed and constructed in the laboratory was used for shear testing, as shown in Fig. 2. The instrument was connected to a universal testing machine (IDW-200H), and the loading rate was 1 μm s<sup>-1</sup>. The positions and dimensions of the samples for impact toughness and shear strength tests are shown in Fig. 1, and the interface was processed in the middle of every bimetal sample. Every mechanical test above was repeated three times with the same conditions at room temperature.

The shear strength was calculated by the formula below:

$$\sigma = \frac{F}{A}$$

where  $\sigma$  denotes the bond strength (MPa),  $F$  denotes the ultimate load (N), and  $A$  denotes the bonding area (mm<sup>2</sup>).

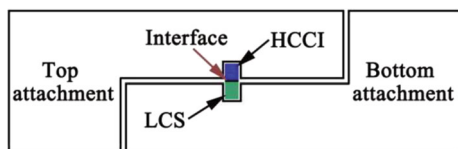
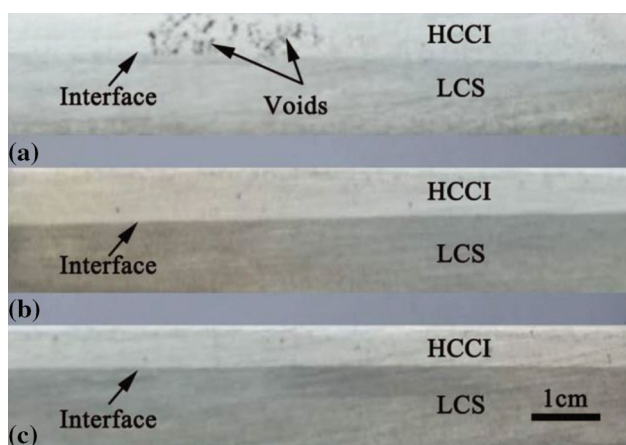
## 3. Results and Discussion

### 3.1 Microstructure

Low-magnification optical micrographs of the bimetals with different holding times are shown in Fig. 3. The HCCI and LCS demonstrated good bonding at different holding times, and a clear and intact interface was observed in the bimetal cross-sections. However, some voids were detected in the HCCI of the sample held for 5 min, which demonstrated that the powder comprising the raw materials cannot fully react in a short holding time, resulting in the formation of defects. Surface liquid-phase sintering requires the powder raw materials to react at 1270 °C, form a liquid alloy and then metallurgically bond to the LCS. However, the insufficient holding time of 5 min did not completely liquefy the alloy, resulting in the appearance of defects in the microstructure of the as-cast HCCI. The microstructure of the samples with a 20 and 40 min

**Table 2 Different heat treatments and sample codes**

Material	Details of treatment	Sample code
HCCI	Quenching (1040°C)	Q1040
Bimetal	Quenching (1040°C)	
	Quenching (1040°C) + Tempering (500°C)	QT500
	Quenching (1040°C) + Tempering (550°C)	QT550
	Quenching (1040°C) + Tempering (600°C)	QT600

**Fig. 2** Schematic illustration of a home-made instrument for shear strength test**Fig. 3** Low-magnification optical micrographs of the bimetal with different holding time: (a) 5 min, (b) 20 min, (c) 40 min

holding time showed excellent bonding quality. The effect of the holding time on the fabrication of a bimetal was demonstrated and holding for 20 min produced an acceptable bimetal material.

Figure 4 shows the OM micrographs of the bonding interface of bimetal with different holding times. The top side panel shows the HCCI, and the bottom side panel shows the LCS. The interface was almost a straight line without any microvoids, microcracks and unbonded regions. On the HCCI side, the microstructure consisted of an  $M_7C_3$  carbide, an  $M_2C$  carbide and a ledeburite matrix (Ref 24). On the LCS side, the pearlite and ferrite gains were large with an average size of 68  $\mu\text{m}$  due to the substantial growth of the grains during the 1270 °C heat treatment process. An off-white ferrite band can be seen near the interface on the LCS side, and an opposite black narrow band can be seen on the HCCI side, which can be referred to as the diffusion zone. The details of the black band are shown in Fig. 4(d); it can be identified as troostite with fine lamellar carbides distributed in the ferrite matrix.

The BF-TEM micrograph of the diffusion zone is shown in Fig. 5(a). The lamellar carbide was identified as  $M_3C$  by the corresponding SADP. The TEM-EDS analysis of  $M_3C$  is shown

in Fig. 5(b), and its Fe/M (Cr, Mo) atom ratio was calculated as 3.0. Based on our previous study, the microstructure of the diffusion zone was studied in a diffusion couple consisting of the HCCI (16 wt.% Cr with no addition of Mo) and the LCS. The results showed that the carbide type in the diffusion zone was  $M_{23}C_6$ , and the spacing of the  $M_{23}C_6$  lamellar was 63 nm on average (Ref 22). The addition of Mo is the reason for the formation of this microstructure in the present study, and it affected the stability of the austenite at high temperatures and changed the solidification process. The Mo atoms dissolved in the austenite by replacing the Cr atoms and delayed the transformation of the austenite to pearlite (Ref 25).

EPMA was used to analyze the diffusion zone of the sample held for 20 min to investigate the diffusion of the atoms on the interface, and the result is shown in Fig. 6. In our previous research (Ref 22), C atoms diffused from the LCS to the HCCI, which can be considered as uphill diffusion; the diffusion of the Cr atoms cannot occur due to their large atomic diameter. The results of Fig. 6 agree with that assessment, and a C-poor ferrite zone formed because the C atoms diffused from the LCS to the HCCI, and the diffusion of the Mo and Cr atoms did not occur because they were not detected in the LCS side (Fig. 6(c) and (d)). According to the hypothesis by L. Shi (Ref 26), the diffusion driving force originates from the chemical potential gradient, and Cr and Mo reduced the chemical potential of C atoms in the Fe-Cr-C and Fe-Mo-C ternary systems, respectively. In the present study, the effect of the Cr and Mo in reducing the chemical potential of the C was superimposed. Compared with our previous research (Ref 22), the chemical potential of C was further decreased, and then, the driving force of the uphill diffusion was increased.

Upon comparing the width of the ferrite band in the samples held for different times in Fig. 4, it can be seen that the width of the ferrite band did not increase with increasing holding time. This is due to two factors. On the one hand, as the diffusion of C atoms continued, the C content in the diffusion zone increased, leading to an increase in the chemical potential of the C and decreasing the diffusion driving force. On the other hand, in the early stage of the diffusion, the C-poor ferrite band gradually widened, and the driving force needed for the diffusion of C atoms increased. When the driving force provided by the chemical potential gradient was balanced by the driving force required for the long-range diffusion of the C atoms, the diffusion behavior ended. The width of the ferrite band and diffusion zone remained unchanged.

### 3.2 Microhardness

The microhardness near the interface of the sample held for 20 min (before and after heat treatments) is shown in Fig. 7. The microhardness in the as-cast sample on the LCS side was

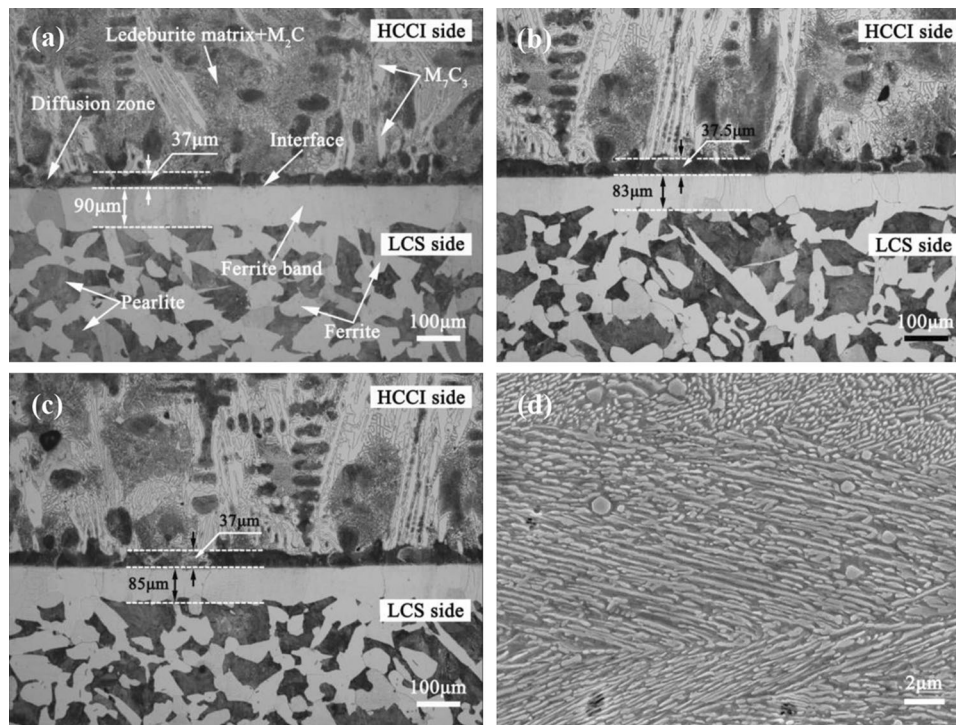


**Fig. 4** OM micrographs of the bonding interface of bimetal with different holding time: (a) 5 min, (b) 20 min, (c) 40 min; (d) SEM detail of the diffusion zone of the holding 20 min sample

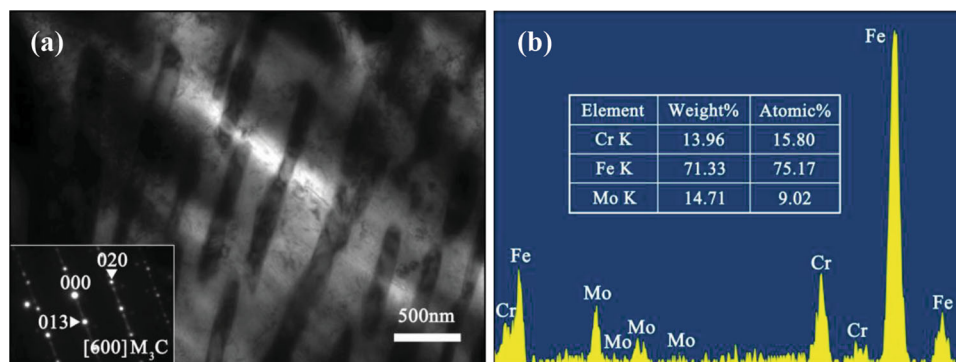


**Fig. 5** BF-TEM micrograph of the diffusion zone of the 20 min holding time sample and corresponding SADP

low due to the formation of a C-poor ferrite band with a width of 83  $\mu\text{m}$  by the interface, and a slight increase was noticed out of that range. On the HCCI side, the microhardness obviously increased. The high Cr and Mo content of the carbides in the diffusion zone improved the solid solution strengthening; the microhardness sequentially increased, attributed to the hard  $\text{M}_7\text{C}_3$  and Mo-rich carbides in the microstructure of the HCCI. For the sample that was heat treated and destabilized, the LCS uniformity increased during the soaking process and showed similar microhardness values after the forced air cooling. On the HCCI side, the microhardness obviously increased due to the formation of martensite with high C content in the diffusion zone, and the microhardness of the HCCI was also high because of a microstructure that consisted of hard carbides and a martensite matrix with secondary carbides. After the tempering treatment, the microhardness did not show an obvious change on the LCS side compared with the sample that underwent a destabilization heat treatment; however, because of

the exsolution of the C and alloy atoms in the martensite matrix, the microhardness of the tempered samples decreased with increasing tempering temperature on the HCCI side. The microhardness of the HCCI increased in the diffusion zone in every tempered sample, which was due to a high C content in the diffusion zone, which retained a volume fraction of martensite, leading to the high microhardness after tempering treatments.

### 3.3 Impact Toughness

The toughness of HCCI samples decreased with an increase in the abrasive resistance by the addition of alloying elements. In the present study, LCS with good toughness can improve the impact resistance of the bimetal, and the results after the impact test are shown in Fig. 8. The toughness of bimetal is much higher than that of HCCI under the as-cast condition. After forced air cooling treatment, the impact toughness of HCCI

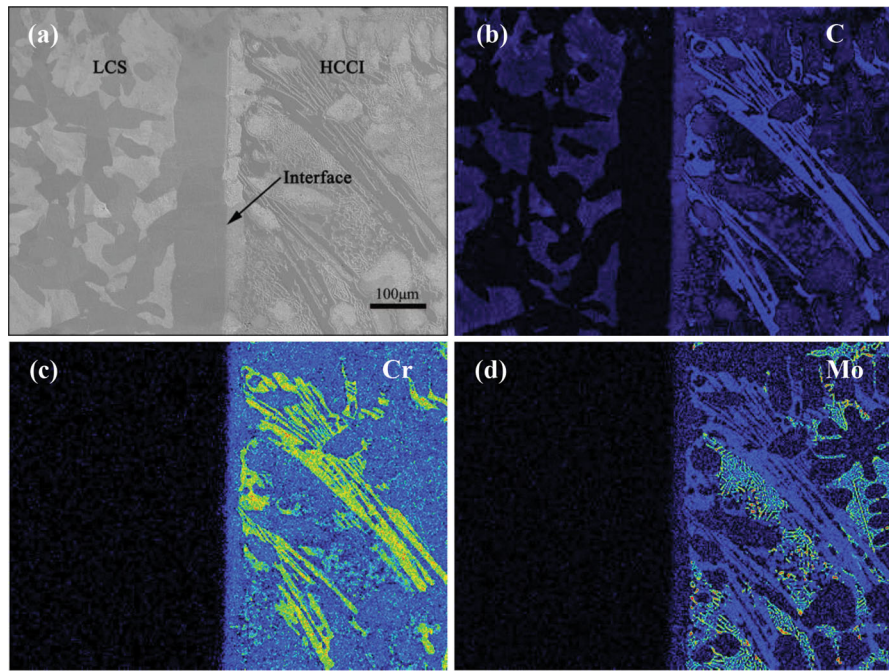


**Fig. 6** EPMA micrographs of the bonding interface: (a) Compo-image, (b) C distribution image, (c) Cr distribution image, (d) Mo distribution image

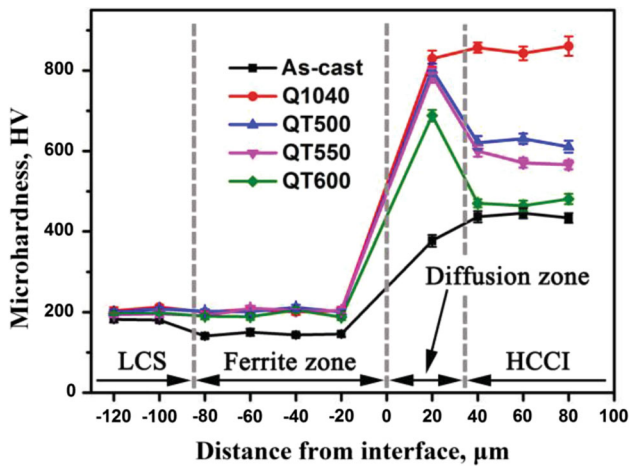


**Fig. 7** Variation of microhardness as a function of distance from the interface

decreased because of the brittleness caused by martensite transformation of matrix. The grain size of the LCS excessively increased during the furnace cooling process, causing a decrease in the tensile strength of the as-cast LCS, resulting in a lower impact toughness of the bimetal. The impact toughness increased after forced air cooling because of the increase in the LCS strength (Fig. 7). After tempering treatment, the martensitic brittleness was eliminated, leading to the improvement of impact toughness of the tempered samples, and it increased with an increase in the tempering temperature.

### 3.4 Shear Strength

The shear strength can accurately reflect the bonding strength of a bimetal, and the results from this study are shown in Fig. 9. As discussed above, the width of the ferrite band and

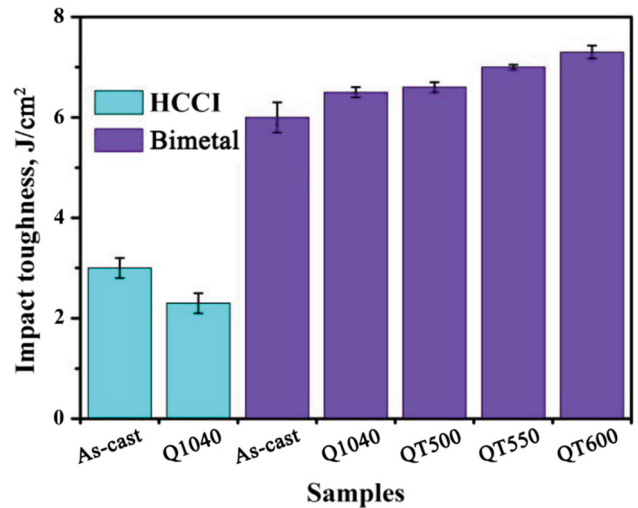


**Fig. 8** Impact toughness of the as-cast and heating treated HCCI and bimetal samples

diffusion zone remained almost unchanged with increasing holding time, leading to nearly the same shear strength. In the HCCI/medium carbon steel (MCS) diffusion couple in the research by B. Xiong, the shear strength improved with increasing liquid–solid volume ratio and peaked at approximately 260 MPa (Ref 16). In the research by B. Kurt, the shear strength of the gray cast iron/MCS bimetal decreased with decreasing bonding temperatures, and the highest value (142 MPa) was produced at the test temperature of 1000 °C (Ref 18). Gao fabricated a HCCI/LCS bimetal by hot diffusion compression bonding, and the optimal shear strength in his research was approximately 315 MPa (Ref 21). Compared with the above works, the bimetal fabricated in this study has the advantage of bonding strength.

SEM fractographs of shear testing samples with different holding times are shown in Fig. 10. There is no obvious difference in the fractograph features of samples with various holding times; all fractographs comprise shear bands and shear dimples. The fractograph of the sample held for 40 min shows the characteristics of a toughening nest.

Shear strength values for the sample held for 20 min with various heat treatment conditions are shown in Fig. 11. The shear strength of the sample after heat treatment significantly decreased compared with that of the as-cast sample (586.2 MPa, shown in Fig. 9), and had a descending trend with increasing tempering temperature. The shear strength of the QT600 sample was as low as 358.9 MPa.

To analyze the reason for the shear strength decrease after heat treatment, SEM micrographs of the diffusion zone of the

as-cast and Q1040 samples were obtained and are shown in Fig. 12. In our previous research (Ref 22), the HCCI grains grew along the orientation of the LCS grains during the solidification process. This led to the formation of grain boundaries across the interface, which could effectively improve the shear strength. These results of this study are consistent with those findings because a grain boundary can be seen across the interface, as shown in Fig. 12(a). However, the Q1040 sample had an entirely different interface microstructure, and the grain boundary was along the interface, as shown in Fig. 12(b). Due to the different components in the HCCI and LCS, their grain orientations changed during the forced-air cooling that occurred after austenitizing. The grain boundaries coincided with the interface. When the sample was subjected to

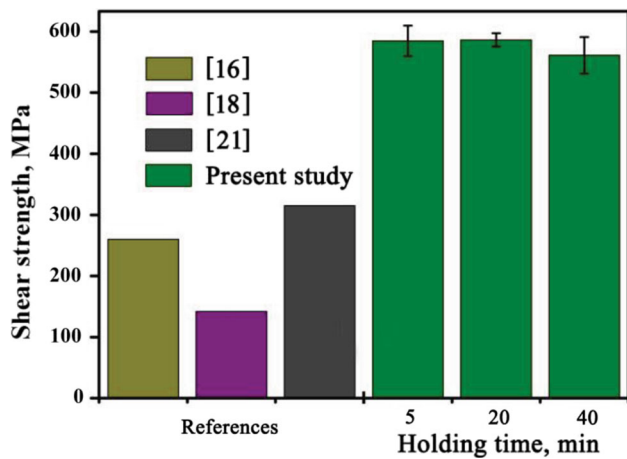


Fig. 9 Variation of shear strength of several works

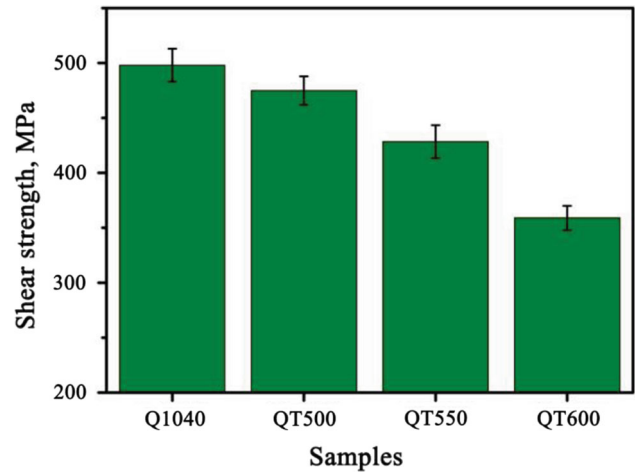


Fig. 11 Shear strength of bimetal samples with different heat treatment conditions

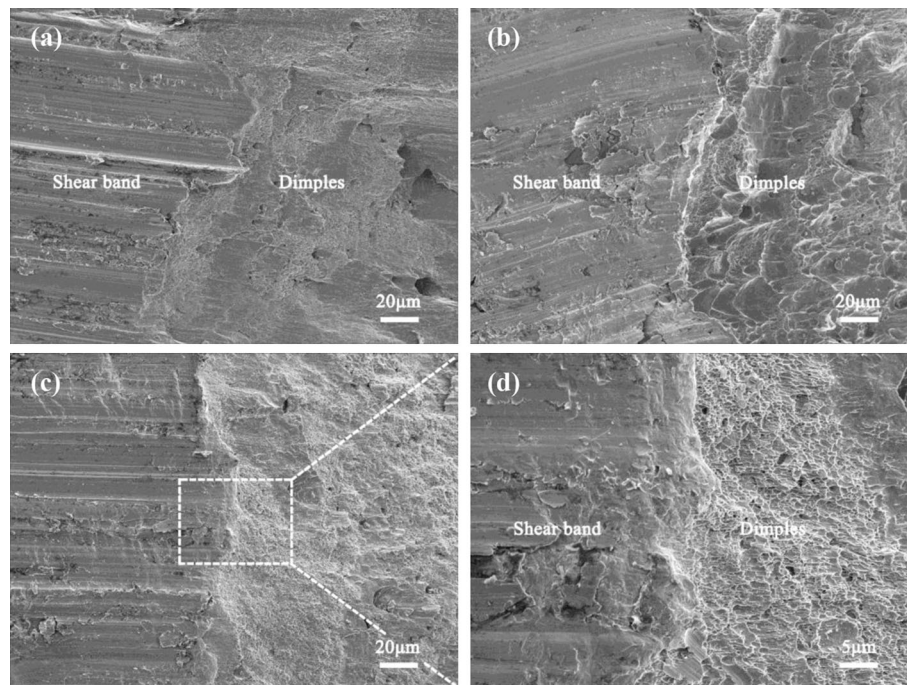
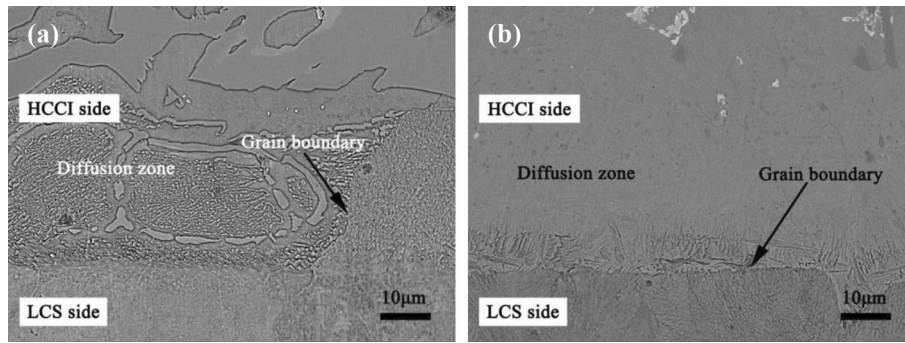
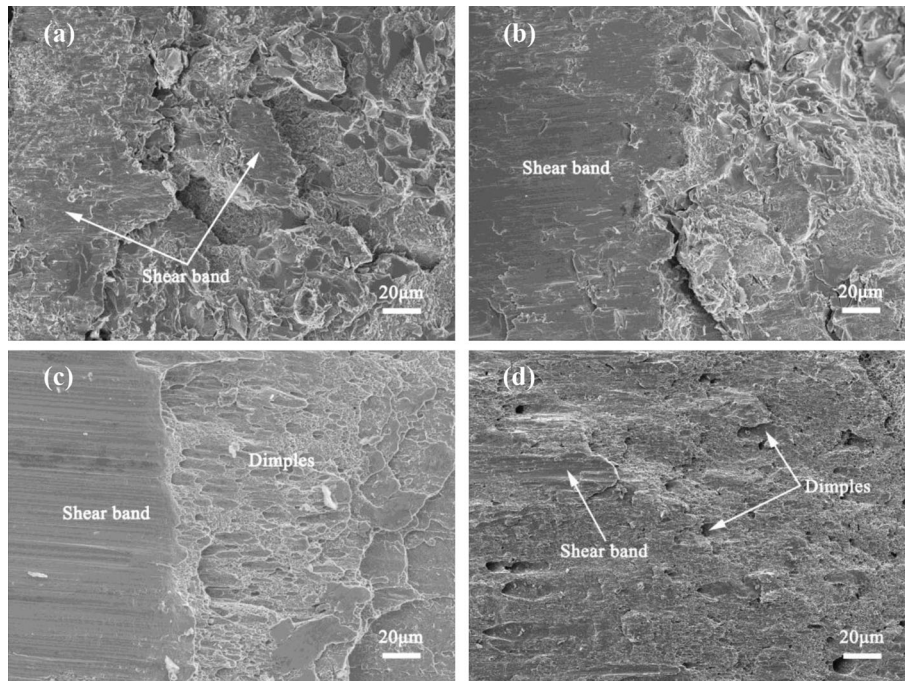


Fig. 10 SEM fractographs of shear testing samples with different holding time: (a) 5 min, (b) 20 min, (c) 40 min, (d) Detail of holding 20 min sample



**Fig. 12** SEM micrographs of the diffusion zone of as-cast and heat treatment sample: (a) As-cast sample, (b) Q1040 sample



**Fig. 13** SEM fractographs of shear strength test samples with different heat treatment: (a) Q1040 sample, (b) QT500 sample, (c) QT550 sample, (d) QT600 sample

a shear force during the shear testing, sliding easily occurred along these grain boundaries, resulting in a decrease in the shear strength. After the tempering treatment, the supersaturated solid solubility of the martensite in the diffusion zone further decreased, and the crystal mismatch with the LCS increased, leading to a decrease in the shear strength with increasing tempering temperature.

SEM fractographs of shear strength test samples after heat treatment are shown in Fig. 13. The SEM fractograph of the Q1040 sample presents obvious cleavage fracture characteristics because of the quenching stress and martensitic brittleness at the interface that was produced during the quenching process. The shear band is discontinuous, which is indicative of brittleness. As the temperature increased, the shear band became more complete, and the dimples began to protrude.

## 4. Conclusions

In the present study, HCCI was bonded to LCS by surface liquid-phase sintering, and the bimetal was subjected to a quenching + tempering treatment. The microstructure of the bimetal was analyzed by OM, SEM, EMPA and TEM. The mechanical properties were characterized by microhardness, impact and shear tests. The following conclusions can be summarized:

1. The HCCI showed good bonding with the LCS with no defects, such as voids, cracks, and unbonded regions, present in the samples with holding times of at least 20 min. The sample held for 5 min showed uncompacted structures in the HCCI.

2. The uphill diffusion phenomenon of C atoms occurred between the HCCI and LCS, and a diffusion zone was formed by the interface on the HCCI side. The width of the diffusion zone remained unchanged with increased holding times and maintained a value of approximately 37  $\mu\text{m}$ .
3. The impact toughness of the bimetal was significantly improved compared with that of the HCCI. After quenching treatment, the microhardness of the diffusion zone improved, and the impact toughness of the bimetal decreased. For the tempered samples, the microhardness decreased, and the impact toughness increased with increasing tempering temperature.
4. The different holding times had no obvious influence on the bonding strength of the samples, which both showed high values. There was a reduction in the shear strength of the quenched sample, and it continuously decreased as the tempering temperature increased.

## Acknowledgments

This research was supported by the National High Technology Research and Development Program (2012AA03A508), and the National Natural Science Foundation of China (U1360102 and 51275344).

## Conflict of interest

The authors declare no conflict of interest.

## References

1. C.P. Tabrett, I.R. Sare, and M.R. Ghomashchi, Microstructure-Property Relationships in High Chromium White Iron Alloys, *Int. Mater. Rev.*, 1996, **41**, p 59–82
2. K.D. Tozetti, E. Albertin, and C. Scandian, Abrasive Size and Load Effects on the Wear of a 19.9% Chromium and 2.9% Carbon Cast Iron, *Wear*, 2017, **376–377**, p 46–53
3. Ö.N. Doğan and J.A. Hawk, Effect of Carbide Orientation on Abrasion of High Cr White Cast Iron, *Wear*, 1995, **189**, p 136–142
4. Ö.N. Doğan, J.A. Hawk, and G. Laird, II, Solidification Structure and Abrasion Resistance of High Chromium White Irons, *Metall. Mater. Trans. A*, 1997, **28A**, p 1315–1328
5. C. Scandian, C. Boher, J.D.B. de Mello, and F. Rézai-Aria, Effect of Molybdenum and Chromium Contents in Sliding Wear of High-Chromium White Cast Iron: The Relationship Between Microstructure and Wear, *Wear*, 2009, **267**, p 401–408
6. K. Shimizu, K. Kusumoto, X. Yaer, Y. Zhang, and M. Shirai, Effect of Mo Content on Erosive Wear Characteristics of High Chromium Cast Iron at 1173 K, *Wear*, 2017, **376–377**, p 542–548
7. J.J. Penagos, J.I. Pereira, P.C. Machado, E. Albertin, and A. Sinatora, Synergetic Effect of Niobium and Molybdenum on Abrasion Resistance of High Chromium Cast Irons, *Wear*, 2017, **376–377**, p 983–992
8. A.E. Karantzalis, A. Lekatou, and H. Mavros, Microstructural Modifications of As-Cast High-Chromium White Iron by Heat Treatment, *J. Mater. Eng. Perform.*, 2009, **18**, p 174–181
9. J. Wang, C. Li, H. Liu, H. Yang, B. Shen, S. Gao, and S. Huang, The Precipitation and Transformation of Secondary Carbides in a High Chromium Cast Iron, *Mater. Charact.*, 2006, **56**, p 73–78
10. M. Zhang, P.M. Kelly, and J.D. Gates, The Effect of Heat Treatment on the Toughness, Hardness and Microstructure of Low Carbon White Cast Irons, *J. Mater. Sci.*, 2001, **36**, p 3865–3875
11. G. Hu, H. Meng, and J. Liu, Microstructure and Elevated Temperature Wear Behavior of Induction Melted Fe-Based Composite Coating, *Appl. Surf. Sci.*, 2014, **317**, p 378–384
12. F. Ye, M. Hojamberdiev, Y. Xu, L. Zhong, N. Zhao, Y. Li, and X. Huang, Microstructure, Microhardness and Wear Resistance of VCp/Fe Surface Composites Fabricated In Situ, *Appl. Surf. Sci.*, 2013, **280**, p 297–303
13. K.K. Chang, S. Lee, and J.Y. Jung, Effects of Heat Treatment on Wear Resistance and Fracture Toughness of Duo-Cast Materials Composed of High-Chromium White Cast Iron and Low-Chromium Steel, *Metall. Mater. Trans. A*, 2006, **37A**, p 633–643
14. H. Oh, S. Lee, J.Y. Jung, and S. Ahn, Correlation of Microstructure with the Wear Resistance and Fracture Toughness of Duocast Materials Composed of High-Chromium White Cast Iron and Low-Chromium Steel, *Metall. Mater. Trans. A*, 2001, **32A**, p 515–524
15. X. Xiao, S. Ye, W. Yin, and Q. Xue, HCWCI/Carbon Steel Bimetal Liner by Liquid-Liquid Compound Lost Foam Casting, *J. Iron Steel Res. Int.*, 2012, **19**, p 13–19
16. B. Xiong, C. Cai, and B. Lu, Effect of Volume Ratio of Liquid to Solid on the Interfacial Microstructure and Mechanical Properties of High Chromium Cast Iron and Medium Carbon Steel Bimetal, *J. Alloys Compd.*, 2011, **509**, p 6700–6704
17. B. Xiong, C. Cai, H. Wan, and B.P. Lu, Fabrication of High Chromium Cast Iron and Medium Carbon Steel Bimetal by Liquid-Solid Casting in Electromagnetic Induction Field, *Mater. Des.*, 2011, **32**, p 2978–2982
18. B. Kurt, N. Orhan, and A. Hasçalık, Effect of High Heating and Cooling Rate on Interface of Diffusion Bonded Gray Cast Iron to Medium Carbon Steel, *Mater. Des.*, 2007, **28**, p 2229–2233
19. M. Eroglu and B. Kurt, Diffusion Bonding Between High Chromium White Iron and Low Carbon Steel, *Mater. Sci. Technol.*, 2007, **23**, p 171–176
20. H. Wang and S. Yu, Influence of Heat Treatment on Microstructure and Sliding Wear Resistance of High Chromium Cast Iron Electroslag Hardfacing Layer, *Surf. Coat. Technol.*, 2017, **319**, p 182–190
21. X. Gao, Z. Jiang, D. Wei, S. Jiao, D. Chen, J. Xu, X. Zhang, and D. Gong, Effects of Temperature and Strain Rate on Microstructure and Mechanical Properties of High Chromium Cast Iron/Low Carbon Steel Bimetal Prepared by Hot Diffusion-Compression Bonding, *Mater. Des.*, 2014, **63**, p 650–657
22. Y. Li, M. Gong, K. Wang, P. Li, X. Yang, and W. Tong, Diffusion Behavior and Mechanical Properties of High Chromium Cast Iron/Low Carbon Steel Bimetal, *Mater. Sci. Eng. A*, 2018, **718**, p 260–266
23. W. Tong, Y. Li, K. Wang, A novel method for preparing bimetal composite material by surface liquid sintering technology, 201710566299.0 (2017) (Patent, in Chinese)
24. Y. Li, P. Li, K. Wang, H. Li, M. Gong, and W. Tong, Microstructure and Mechanical Properties of a Mo Alloyed High Chromium Cast Iron After Different Heat Treatments, *Vacuum*, 2018, **156C**, p 59–67
25. S. Inthidech, P. Sricharoenchai, and Y. Matsubara, Effect of Sub-critical Heat Treat Parameters on Hardness and Retained Austenite in Mo Containing High Chromium Cast Irons, *Int. J. Metalcast.*, 2012, **6**, p 25–34
26. L. Shi, *Thermodynamics of Alloys*, 11th ed., China Machine Press, Beijing, 1992, p 316–414 ((in Chinese))

**Publisher's Note** Springer Nature remains neutral with regard to jurisdictional claims in published maps and institutional affiliations.